*Int. J. Electrochem. Sci.*, 13 **(2018)** 9731 – 9741, doi: 10.20964/2018.10.27

International Journal of
ELECTROCHEMICAL
SCIENCE
www.electrochemsci.org

# Effect of Microstructure on Corrosion Resistance of Anodic Oxidation Coatings on TA2 Commercially Pure Titanium in Sodium-Tartrate Solution

*Xiao Wang, Ju Rong*[*]*, Yuhan Yao, Jing Feng, Yannan Zhang, Xiaohua Yu*[*]*, Zhaolin Zhan*

Faculty of Materials Science and Engineering, Kunming University of Science and Technology, Kunming, 650093, China
[*]E-mail: JRong_kmust@163.com; xiaohua_y@163.com

*Received:* 25 May 2018 / *Accepted:* 17 July 2018 / *Published:* 1 September 2018

Titanium anodic oxide films were prepared using a constant-potential method in a sodium-tartrate environmentally friendly electrolyte at different concentrations (1, 5, 15, 30 and 50 g $L^{-1}$). The microstructure, elemental composition, and microscopic three-dimensional morphology of the film were analyzed by scanning electron microscopy, energy-dispersive spectrometry, and atomic force microscopy. The polarization curve and electrochemical impedance spectroscopy of the sample at a low potential in 3.5% NaCl solution were studied by using an electrochemical workstation. The effect of the microscopic three-dimensional morphology on the corrosion resistance was discussed. The surface morphology of the oxide film indicates that a uniform and complete oxide film with a lower roughness can be obtained in the 15 g $L^{-1}$ sodium-tartrate solution concentrations. As the sodium-tartrate electrolyte concentrations increases, the depths of the cracks deepen and the size of the raised bulges increases. The resulting oxide film has a wide passivation region of 0 to 4 V, a maximum polarization resistance, a small passivation-induced current value, and a low corrosion current value of $3.730 \times 10^{-5}$ A·$cm^{-2}$, and thus, it exhibits an excellent corrosion resistance, and a wide range of potential applications, such as in biological technologies. This work provides a new approach to prepare environmentally friendly, non-polluting titanium anodic oxide films and proposes a novel design to adjust the corrosion resistance performance of the anodized film.

**Keywords:** TA2 pure titanium; anodic oxidation; corrosion resistance; atomic force microscopy

## 1. INTRODUCTION

In recent years, titanium and titanium alloys have received extensive attention because of their excellent mechanical and chemical properties, and they have been used widely in aerospace, industrial production and biomedical industries [1, 2]. Previous studies show that the excellent properties of

titanium and titanium alloys are related directly to the natural oxide film on its surface [3]. However, the natural oxide film is thin and is easily damaged, which results in a poor corrosion resistance and material wear resistance [4]. Many researchers hope to use a surface-modification technology to generate a denser and a more corrosion-resistant passive film [5]. The most commonly used surface-modification technology for titanium and titanium alloys is the anodizing process [6, 7] (in a specific electrolyte, an oxide film is formed on the surface of the anode-metal material under external power-supply conditions).

Current electrolyte that is used in the anodizing process is mainly acid-based solution, such as sulfuric, phosphoric or oxalic acid. However, previous work has reported that such electrolytes tend to cause hydrogen embrittlement when titanium and titanium alloys are used, and they affect the environment and the human body adversely [8]. Wang et al. prepared $TiO_2$ films on a Ti surface with HF electrolytes that are used in anodizing processes and that contain fluoride ions and chromium ions. However, because fluoride and chromium ions are toxic, they can harm the environment and the human body further [9]. Based on this information, it is of great practical value to study a new type of environmentally friendly anodizing process.

Based on the characteristics of low-potential anodic oxide film that have attracted the attention of researchers in recent years [10], we propose an environmentally friendly, non-polluting, alkaline sodium-tartrate electrolyte. The quality of the titanium anodized film was regulated by the concentration of the electrolyte at a low voltage. Scanning electron microscopy (SEM) and energy-dispersive spectrometry (EDS) were used to analyze the microstructure and elemental composition. Atomic force microscopy (AFM) was used to analyze the effect of sodium-tartrate electrolyte concentration on the morphology and structure of the anodic oxide film. The change in the Tafel polarization curve and electrochemical impedance spectroscopy curve of the anodic oxidation film was measured by an electrochemical workstation. This work aims to elucidate the mechanism of the effect of the microscopic three-dimensional morphology on corrosion resistance of the anodized layer prepared by sodium-tartaric-acid solution with a low potential, provides a basis for further application of the titanium-oxide film and proposes a novel method of using sodium-tartaric-acid solution concentration to adjust the quality of the anodized film.

## 2. EXPERIMENTAL DETAIL

### *2.1 Preparation of titanium anodic oxide films*

The substrate material was selected from a TA2 pure titanium plate (Youju Group, Japan) with a uniform grain structure. The specific chemical composition is shown in Table 1.

**Table 1.** Chemical composition of TA2 commercially pure titanium

| Element | O | N | C | H | Fe | Si | Ti |
|---|---|---|---|---|---|---|---|
| Mass fraction/% | 0.15 | 0.05 | 0.05 | < 0.015 | < 0.30 | < 0.15 | Bal. |

Titanium sheet was cut to 100 mm × 20 mm × 0.5 mm, and sanded consecutively with 400#,

800# and 1000# sandpaper. Ultrasonic cleaning was performed in a solution of acetone, ethanol and deionized water solution, and the sheet was soaked in deionized water for later use. Before anodizing, electrochemical polishing is also required. The polishing solution was a mixture of sodium tartrate, methanesulfonic acid and deionized water.

The polished titanium plate was cleaned in deionized water, dried in an oven and anodized. The anodized power supply was a IPD-20001SLU-type constant-voltage direct-current power supply. The sodium-tartrate concentrations were 1, 5, 15, 30 and 50 g $L^{-1}$, respectively (according to the oxidation process). A schematic of the titanium anodizing is shown in Fig. 1. The anode is TA2 pure titanium plate, the cathode is a graphite plate, the area ratio of the cathode to the anode is 2:1 and the distance between the electrodes is 5 cm. The test temperature was 25°C, the oxidation time was 1800 s and the voltage was 10 V.

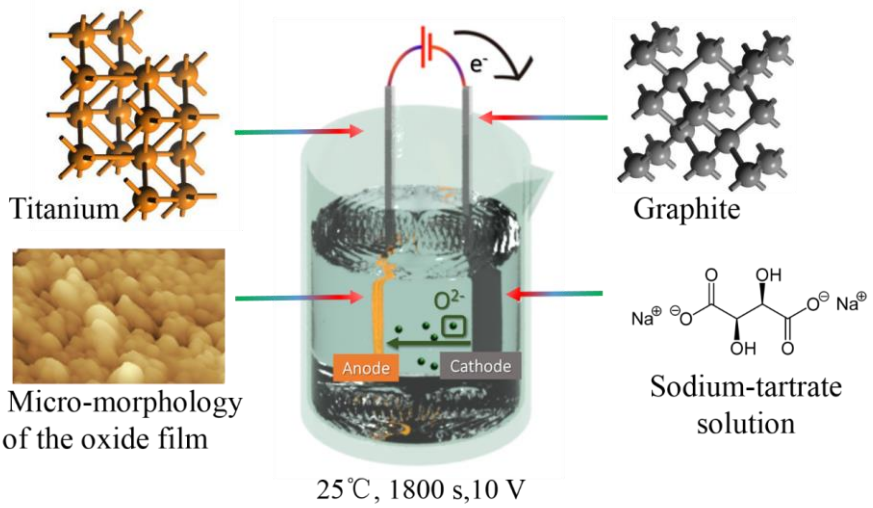


**Figure 1.** Titanium anodizing schematic.

*2.2 Materials characterization and electrochemical measurements*

The auxiliary electrode was a platinum electrode, the working electrode was anodized TA2 pure titanium sample, the working area was 1 cm2, the dielectric was 3.5% NaCl solution and the test temperature was room temperature (25°C). For the polarization-curve measurement, the initial potential was set to –4 V, the termination potential was 4 V and the scan speed was 1 mV $s^{-1}$. Before the electrochemical impedance spectroscopy measurement, the open potential of the working electrode was measured and the open circuit potential reached stability before the impedance test was performed. The amplitude of the measured sine wave AC excitation signal was ±5 mV and the frequency range was $10^{5}$–$10^{-2}$ Hz. The scanning step was 5°.

## 3. RESULTS AND DISCUSSION

*3.1 Micromorphology*

The surface morphologies of the anodized films prepared with different sodium-tartrate

electrolyte concentrations (1, 5, 15, 30 and 50 g $L^{-1}$) are shown in Fig. 2. Under low-magnification conditions, the oxide film surface is cracked and bulges convexly. As the sodium-tartrate concentration increases, the depth of the crack deepens, and the size of the raised bulge increases. When the concentration was increased to 30 and 50 g $L^{-1}$, the bulging size increased significantly.

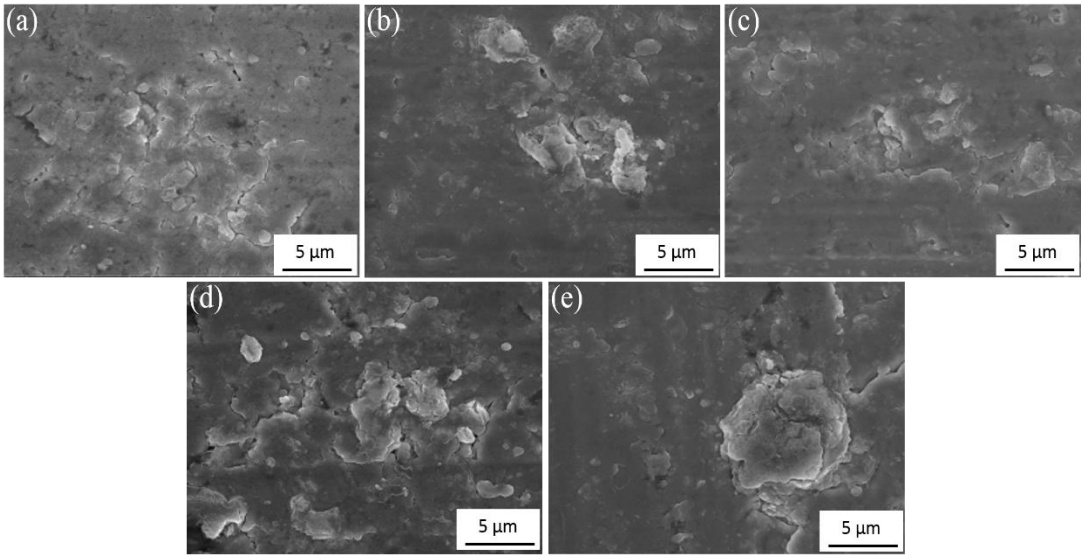


**Figure 2.** SEM images of the anodic oxide film formed at different sodium-tartrate concentrations.

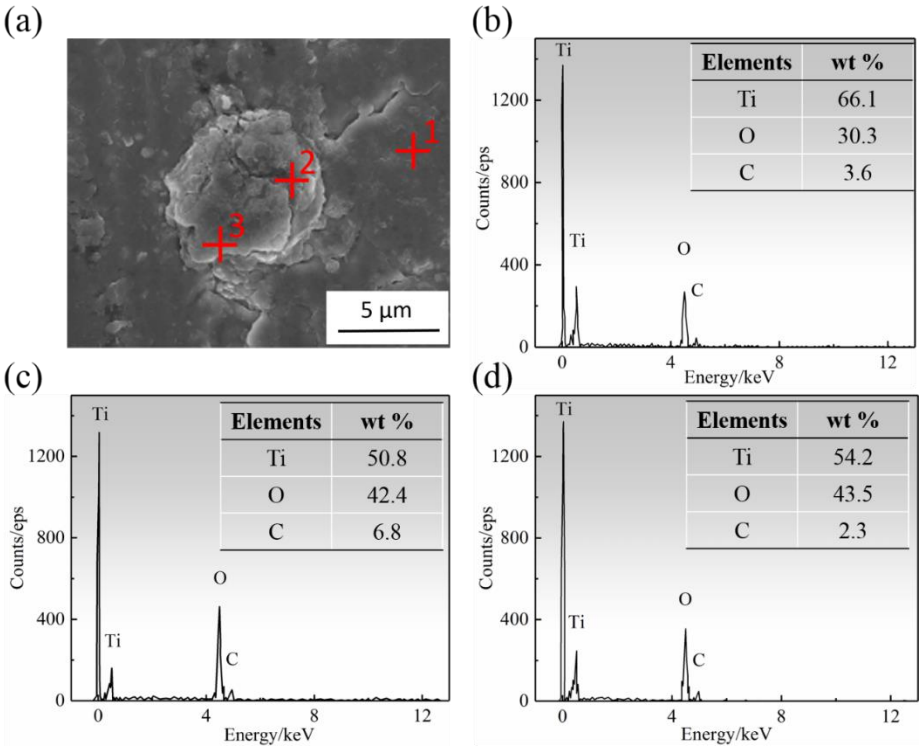


**Figure 3.** EDS images of the anodic oxide film at sodium-tartrate concentration of 15g $L^{-1}$: (b) spectrogram 1, (c) spectrogram 2 and (d) spectrogram 3.

The growth of these bulges may result because of different growth rates in different areas of the oxide film. According to the literature [12], an anodic oxidation film first forms a barrier layer, and when the voltage increases, breakdown occurs and the barrier layer breaks. The outer layer film will be easier to grow on these cracked defective surfaces. As the anodization process continues, the thickness of the oxide film grown at these defects will be thicker than that in other regions. The difference in thickness causes stress inside the oxide film, and the internal stress results in the formation of cracks in the bulge.

Figure 3 shows an EDS dot scan of an anodized film formed in a 15 g $L^{-1}$ sodium tartrate solution, and (b), (c) and (d) correspond to points (1), (2) and (3) in the scan. Figure 3b is a relatively flat, non-bulging area. The energy spectrum analysis results show that the mass percentage of Ti and oxygen is 2:1, and the oxygen content is lower, which indicates that the degree of titanium oxidation is low. The spectrum analysis of the bulge in Figure 3c and 3d shows that the oxygen content increases at this time, and makes the mass percentage of Ti and O approximately 1:1. At the bulge, the anodic oxidation of titanium is even higher.

Figure 4 shows the three-dimensional microstructure of anodized film prepared at different concentrations of sodium-tartrate electrolyte. The oxide film shows large undulations, gullies and spherical particles, which indicate that under similar anodizing conditions, the electrolyte characteristics have a significant influence on the oxide-film micromorphology. It is meaningful to study the micromorphology of the oxide film (similar to the anodizing conditions, the phase composition and surface elements are basically the same, with the difference being in the three-dimensional film shape, but current literature does not focus on this issue [13-15]).

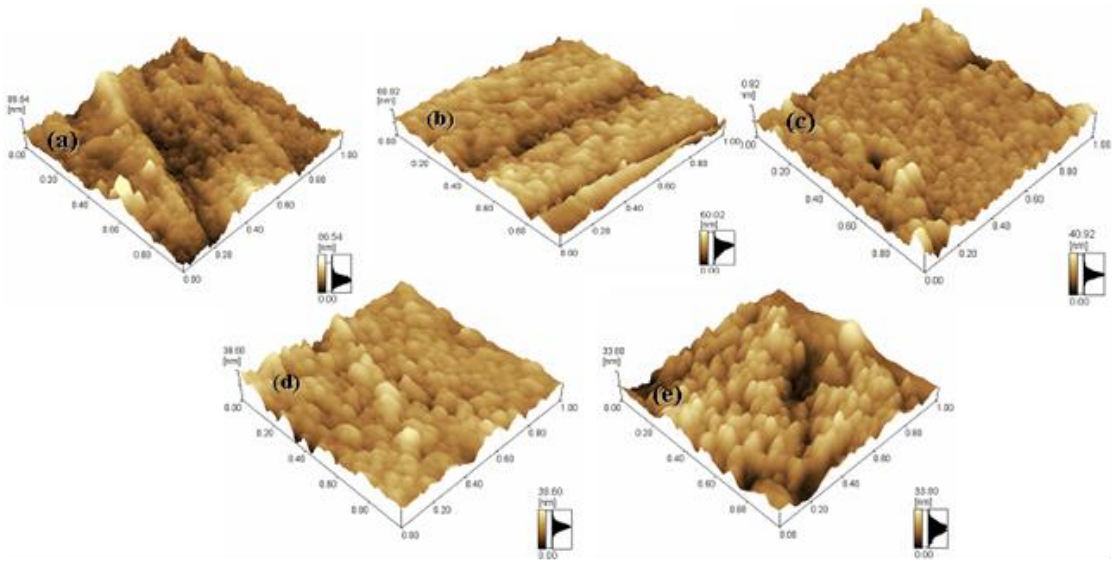


**Figure 4.** AFM images of the anodic oxide film formed at different sodium-tartrate concentrations: (a) 1 g $L^{-1}$, (b) 5 g $L^{-1}$, (c) 15 g $L^{-1}$, (d) 30 g $L^{-1}$, and (e) 50 g $L^{-1}$.

Figure 4a shows that the surface of the oxide film obtained at 1 g $L^{-1}$ forms peaks and valleys with high and low undulations, and local areas contain fine and uniform particles. The film obtained at

5 g $L^{-1}$ did not show large undulations compared with Fig. 4a. Although the overall morphology was particles, the particle size was extremely uneven, as shown in Fig. 4b. The film obtained at 15 g $L^{-1}$ has a more uniform granular structure and the particles are smaller, but a small number of holes appear, as shown in Fig. 4c. When the concentration increased to 30 g $L^{-1}$ (Fig. 4d), the granular structure on the film surface begins to increase laterally, and only the particle size in the local area is uniform. In Fig. 4e, larger and deeper holes appeared in the layer structure obtained at 50 g $L^{-1}$, and the particles also showed a sharp increase in the longitudinal direction.

To show the three-dimensional microscopic morphology of the anodized film layer, the average roughness (Ra) and root-mean-square roughness (Rq) of the film layer are presented in Fig. 5. The roughness of the anodized film layer decreases gradually with an increase in concentration, reaches the lowest point of 15 g $L^{-1}$ and then increases with an increase in concentration.

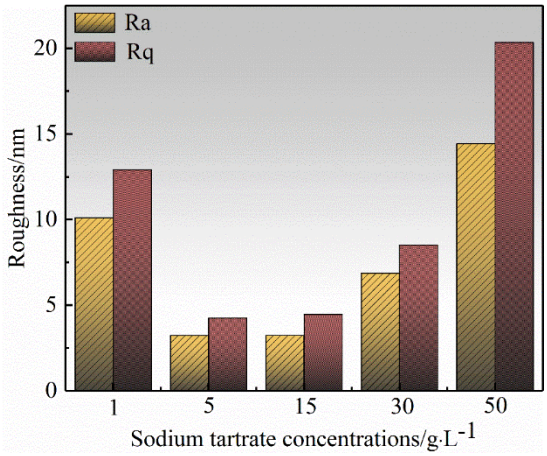


**Figure 5.** Roughness of the anodic oxide film fabricated at different concentrations.

This behavior results because the oxide film growth is limited by concentration at 1 g $L^{-1}$, which results in incomplete film growth, and so the roughness is large [16,17]. When the concentration is increased gradually, the film roughness is reduced because of the complete and uniform growth of the oxide film [18]. As the concentration is increased further, solute ions may accumulate in local areas of the solution. Where the solution ions accumulate, the growth rate of the oxide film is faster than that of the remaining solution [19], which results in an uneven microstructure (Fig. 4d, 4e). The surface roughness of the film layer also increases. These results indicate that the surface morphology of the oxide film obtained at 15 g $L^{-1}$ was fine and uniform, the roughness was low and the film growth was relatively complete.

### *3.2 Electrochemical properties*

Figure 6 shows the potentiodynamic polarization curves of TA2 pure titanium anodic oxide film prepared at different sodium-tartrate solution concentrations. The relevant corrosion-resistance parameters can be obtained from the curves. The specific values are shown in Table 2. The polarization

curves of the five polarizations are approximately the same, and the main reaction in the cathode layer is the hydrogen-evolution reaction.

From –4 to –1.3 V, five curves overlap. From –1.3 V to $E_{corr}$ (corrosion potential), the current density decreases slowly with an increase in potential, which indicates that the hydrogen-evolution rate decreases gradually [20]. When the potential exceeds $E_{corr}$, the titanium plate enters the anode region. The $E_{corr}$ to 0 V region is the activation–passivation region. In this region, the current density increases gradually with an increase in potential. For the polarization curve of the film obtained at 1, 5, 30 and 50 g $L^{-1}$, the 0–1 V region exists in the passivation region. In this region, the current density remains unchanged, and the current that corresponds to this current density is the Insensitive current ($I_{pass}$). The dimensionless blunt current represents the corrosion rate of the passive metal when the anode is protected. A smaller blunt current yields a slower corrosion rate [21]. When the potential exceeds 1 V, the current density starts to increase slightly with an increase in potential, that is, the membrane begins to dissolve and enters the passivation zone [22]. The polarization curve of the film obtained at 15 g $L^{-1}$ showed a wide passivation zone (0 to 4 V) and no passivation zone appeared, which indicates that a pure titanium matrix offers better protection than the anodized film layer that was prepared at 15 g $L^{-1}$.

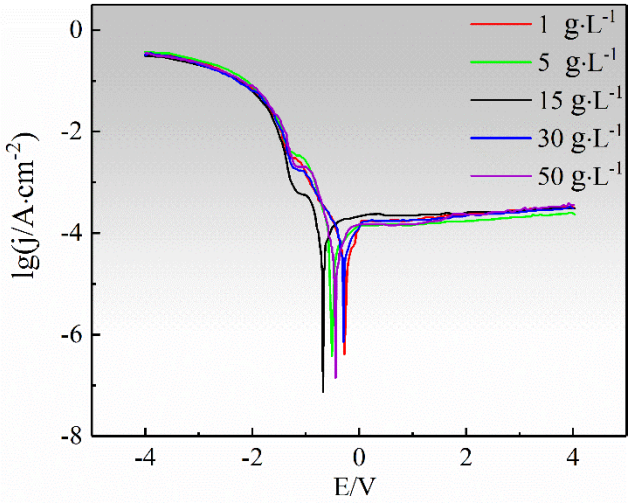


**Figure 6.** Potentiodynamic polarization plots of the anodic titanium-oxide film formed at different sodium-tartrate concentrations in 3.5 wt% NaCl solution.

**Table 2.** Electrochemical parameters obtained from potentiodynamic polarization curves

| Sodium-tartrate concentrations | Ecorr/mV | Icorr/A·cm$^{-2}$ | Ipass/A·cm$^{-2}$ |
|---|---|---|---|
| 1 g L$^{-}$ | –0.269 | $2.620 \times 10^{-5}$ | $1.68 \times 10^{-4}$ |
| 5 g L$^{-}$ | –0.054 | $4.839 \times 10^{-4}$ | $1.77 \times 10^{-4}$ |
| 15 g L$^{-}$ | –0.676 | $3.730 \times 10^{-5}$ | $1.92 \times 10^{-4}$ |
| 30 g L$^{-}$ | –0.295 | $3.204 \times 10^{-5}$ | $1.59 \times 10^{-4}$ |
| 50 g L$^{-}$ | –0.046 | $5.029 \times 10^{-4}$ | $1.78 \times 10^{-4}$ |

Table 2 shows that the five-curve blunt current values do not differ greatly. The 5 g $L^{-1}$ corrosion potential (–0.054 V) and the 50 g $L^{-1}$ corrosion potential (–0.046 V) are higher, which

indicates that the corrosion is less prone than the other three curves; however, the corrosion current value of the two curves is higher than the other three curves, which indicates that the corrosion rate is faster in these two curves. The polarization curves of the film obtained at 1, 15 and 30 g $L^{-1}$ have comparable corrosion potentials and corrosion current values.

The above analysis shows that the polarization curve of the film obtained at 15 g $L^{-1}$ has a wider passivation zone, a slower corrosion rate and therefore the best corrosion resistance.

Figure 7 shows the Nyquist curves of titanium anodized film prepared at different sodium-tartrate solution concentrations. All five curves are incomplete arcs, which indicates that the passivation film has a capacitive load [23].

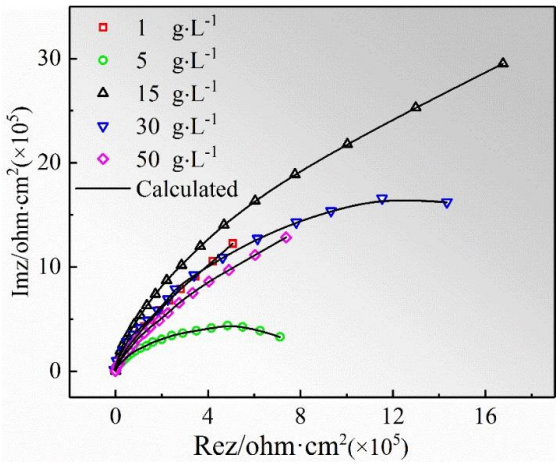


**Figure 7.** Nyquist curves of the titanium anodic-oxide film formed at different sodium-tartrate concentrations.

The arc diameter that corresponds to a concentration of 15 g $L^{-1}$ is the largest. The arc diameter is proportional to the polarization resistance of the film, which means that the film obtained at 15 g $L^{-1}$ has a better corrosion resistance. This result is consistent with the analysis results of the polarization curve.

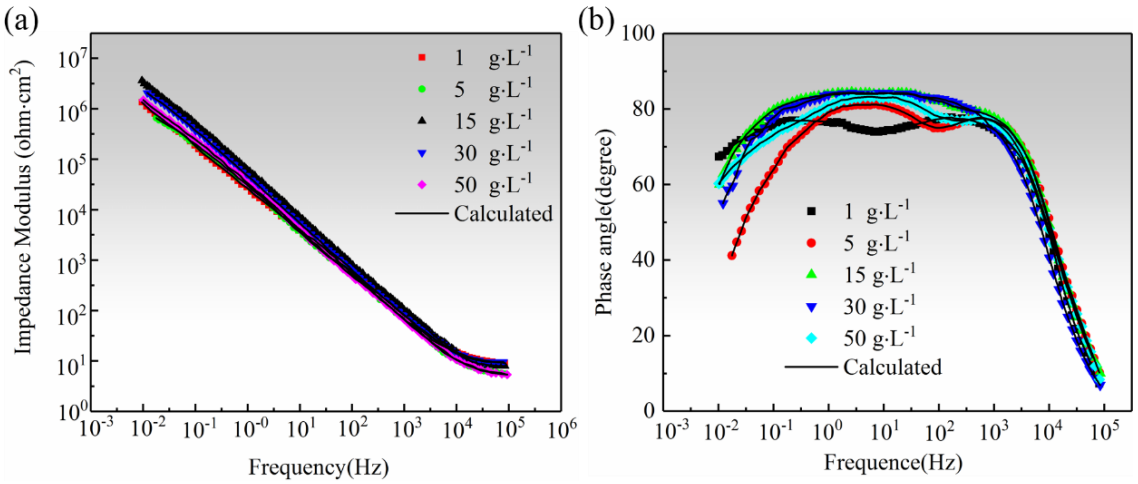


**Figure 8.** Bode curves of the titanium anodic-oxide film formed at different sodium-tartrate concentrations. (a) Bode magnitude plots and (b) Bode phase plots.

Figure 8 shows the Bode amplitude and Bode phase diagrams of the TA2 pure titanium anodic oxidation film prepared at different sodium-tartrate solution concentrations. The curves in Fig. 8a for all curves in the high-frequency region are related to solution resistance [24]. The impedance and frequency in the low to mid frequencies ($10^{-2}$ to $10^{4}$ Hz) exhibit a straight line with a slope of approximately –1, which indicates that the film has a capacitive load [25]. The resistance of the 15 g $L^{-1}$ concentration curve is slightly higher than that of the remaining four, which indicates that it has better corrosion resistance, which is consistent with the analysis result of the previous Nyquist plot.

Figure 8b shows the Bode phase [26-28] diagram of the film. For $10^{-1}$–$10^{3}$ Hz, the phase angles of the film obtained at 5, 15, 30 and 50 g $L^{-1}$ exceed 80° and the maximum is as high as 85°. This result shows that the film obtained in the sodium-tartrate solution above 1 g $L^{-1}$ has a better corrosion resistance.

Figure 8b shows that the curve that corresponds to 15 g $L^{-1}$ has the largest phase angle value in the middle frequency region and the curve has a larger frequency span, which indicates that it has the best protective effect on the titanium substrate [29].

The bilayer membrane structure that is generated on the titanium surface is related (inner and outer membranes) [30]. The time constant that appears in the high-frequency region is related to the formation of the outer porous film. The low-frequency time constant is related to the formation of a dense inner film. Based on this result, the experimental results were fitted using ZSimpWin software [31]. The equivalent circuit was used in the fitting process to study the impedance of the passive film. The equivalent circuit is shown in Fig. 9.

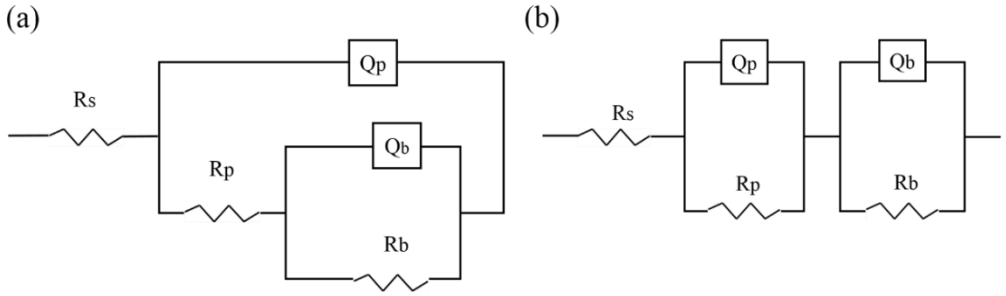


**Figure 9.** Equivalent circuit models ((a) Rs(Qp(Rp(QbRb))) and (b) Rs(QpRp)(QbRb)).

**Table 3.** Electrical parameters of anodic oxide films by fitting using the equivalent circuit

| Parameters | 1 g $L^{-1}$ | 5 g $L^{-1}$ | 15 g $L^{-1}$ | 30 g $L^{-1}$ | 50 g $L^{-1}$ |
|---|---|---|---|---|---|
| $R_S$ ($\Omega \cdot cm^2$) | 7.43 | 5.33 | 7.87 | 9.28 | 5.56 |
| $Q_p \times 10^{-6}$ ($F \cdot cm^{-2}$) | 4.97 | 21.19 | 3.33 | 2.10 | 5.77 |
| $n_p$ | 0.9 | 0.8 | 0.93 | 0.98 | 0.8 |
| $R_p$ ($\Omega \cdot cm^2$) | $1.08 \times 10^4$ | 52.76 | $6.91 \times 10^6$ | 870 | $1.46 \times 10^6$ |
| $Q_b \times 10^{-6}$ ($F \cdot cm^{-2}$) | 2.56 | 6.39 | 5.88 | 1.97 | 3.84 |
| $n_b$ | 0.77 | 0.89 | 1 | 0.85 | 0.8 |
| $R_b$ ($\Omega \cdot cm^2$) | $8.35 \times 10^5$ | $9.24 \times 10^5$ | $1.48 \times 10^6$ | $4.43 \times 10^6$ | $3.15 \times 10^6$ |
| $\chi^2 \times 10^{-4}$ | 2.96 | 2.51 | 3.58 | 3.86 | 1.63 |

The corresponding 5 g $L^{-1}$ film layer is fitted with the equivalent circuit diagram 6b, and the other corresponding film layers are fitted with the equivalent circuit diagram (Fig. 9a). In the

equivalent circuit diagram, RS represents the solution resistance, Qp and Rp represent the equivalent capacitance and resistance of the outer porous membrane, respectively, and Qb and Rb represent the equivalent capacitance and resistance of the dense inner membrane, respectively. The value of the corresponding equivalent circuit can be obtained through ZSimpWin software analysis, as shown in Table 3.

Table 3 shows the error between the fitted and experimental values. The value of $\chi 2$ is very small ($\sim 10^{-4}$), which indicates that the choice of equivalent circuit model is correct. The value of $R_S$ did not change much for the film obtained at different concentrations. The total $R_p$ and $R_b$ of the film obtained at 15 g $L^{-1}$ are much greater than those at the remaining concentrations, which indicates that the film obtained at 15 g $L^{-1}$ has the best corrosion resistance.

## 4. CONCLUSIONS

In this work, titanium anodic oxide films were prepared using a constant-potential method in a sodium-tartrate environmentally friendly electrolyte at different concentrations (1, 5, 15, 30 and 50 g $L^{-1}$). The new environmental anodizing process of sodium tartrate can enhance the titanium corrosion resistance. Polarization-curve study results show that the TA2 pure titanium anodic oxidation film obtained at 15 g $L^{-1}$ has a wider passivation zone, a smaller induced blunt current value and corrosion current value, which indicates that the film layer has a better protective effect on the titanium matrix. Electrochemical impedance spectroscopy test results show that the titanium anodic oxide film obtained at 15 g $L^{-1}$ has the largest polarization resistance value, which indicates that it has the best corrosion resistance. This work provides a new approach to prepare environmentally friendly anodized film with a fine and uniform structure, low roughness, complete film growth and better corrosion resistance.

ACKNOWLEDGEMENTS
This work was supported financially by the National Nature Science Foundation of China (grant Nos. 51601081 and 51665022）

## References

1. R. Asahi, T. Morikawa, T. Ohwaki, K. Aoki and Y. Taga, *Science*, *293*(2001) 269.
2. X. Chen and S. S. Mao, *Chem. Rev*., 107(2007)2891.
3. T. Close, G. Tulsyan, C. A. Diaz, S. J. Weinstein and C. Richter, *Nature Nanotech*., 10(2015)418.
4. L. Benea, E. Mardare-Danaila, M. Mardare and J. P. Celis, *Corros. Sci*., 80(2014)331.
5. M. Fazel, H. R. Salimijazi and M. A. Golozar, *Appl. Surf. Sci.*, 324(2015)751.
6. D. H. Wang, D. Choi, J. Li, Z. G. Yang, Z. M. Nie, R. Kou, D. H. Hu, C. M. Wang, L. V. Saraf, J. G. Zhang, I. A. Aksay and J. Liu, *ACS Nano*, 3(2009)907.
7. P. Roy, B. Steffen and S. Patrik, *Angew. Chem. Int. Ed.*, 50(2011)2904.
8. D. H. Chen, F. Z. Huang, Y. B. Cheng and R. A. Caruso, *Adv. Mater.*, 21(2009)2206.
9. W.Z. Wen, D.R. Jia, Y.Z. Tao, Y.X. Hua, F.T. Lin, Z. Yan, Z.Z. Lin. Int. J. *Electrochem. Sci.*, 13 (2018)4411.
10. F. Zhang, X. H. Liu, C. F. Pan and J. Zhu, *Nanotechnology*, 18(2007)345302.
11. J. H. Lim and J. Choi, *Small*, 3(2007)1504.

12. T. Fu, X. Wang, J. Liu, L. Li, X. Yu and Z. Zhan, *JOM*, 69(2017)1844.
13. H. J. Song, S. H. Park, S. H. Jeong and Y. J. Park, *J. Mater. Process. Technol*. 209(2009)864.
14. M. Shokouhfar, C. Dehghanian, M. Montazeri and A. Baradaran, *Appl. Surf. Sci*., 258(2012)2416.
15. K. H. Kim and N. Ramaswamy, *Dent. Mater. J.*, 28(2009)20.
16. D. D. Macdonald, *Electrochim. Acta*, 56(2011)1761.
17. D. Edström, D. G. Sangiovanni, L. Hultman, I. Petrov, J. E. Greene and V. Chirita, *J. Appl. Phys*., 121(2017)025302.
18. G. S. Frankel, T. Li and J. R. Scully, *J. Electrochem. Soc*., 164(2017) C180.
19. R. Elaish, M. Curioni, K. Gowers, A. Kasuga, H. Habazaki, T. Hashimoto and P. Skeldon, *Electrochim. Acta*, 245(2017)854.
20. S. L. Wang, J. Li, S. Wang, J. E. Wu, T. I. Wong, M. L. Foo, W. Chen, K. Wu and G. Q. Xu, *ACS Catal*., 7(2017)6892.
21. M. M. Rahman, V. G. Alfonso, F. Fabregat-Santiago, J. Bisquert, A. M. Asiri, A. A. Alshehri and H. A. Albar, *Microchim. Acta*, 184(2017)2123.
22. N. Couzon, M. Maillard, L. Bois, F. Chassagneux and A. Brioude, *J. Phys. Chem. C*, 121(2017)22147.
23. Y. Chen, S. Zhao, M. Chen, W. Zhang, J. Mao, Y. Zhao, M. F, Maitz, N. Huang and G. J. Wan, *Corros. Sci.*, 96(2015)67.
24. X. Fu, C. Jia, Z. Wan, X. Weng, J. Xie and L. Deng, *Org. Electron.*, 15(2014)2702.
25. B. Mei, T. Pedersen, P. Malacrida, D. Bae, R. Frydendal, O. Hansen, P. C. K. Vesborg, B. Seger and I. Chorkendorff, *J. Phys. Chem*. C, 119(2015)15019.
26. H. Choi, C. Nahm, J. Kim, J. Moon, S. Nam, D. R. Jung and B. Park, *Curr. Appl. Phys*., 12(2012)737.
27. C. P. Hsu, K. M. , Lee, J. T. W. Huang, C. Y. Lin, C. H. Lee, L. P. Wang, S. Y. Tsai and K. C. Ho, EIS analysis on low temperature fabrication of TiO2 porous films for dye-sensitized solar cells. *Electrochim. Acta*, 53(2008)7514.
28. K. M. Lee, V. Suryanarayanan and K. C. Ho, *J. Power Sources*, 188(2009)635
29. K. Fan, T. Peng, B. Chai, J. Chen and K. Dai, *Electrochim. Acta*, 55(2010)5239.
30. G. Dai, L. Zhao, J. Li, L. Wan, F. Hu, Z. Xu, B. H. Dong, H. B. Lu, S. M. Wang and J. Yu, *J. Colloid Interface Sci*., 365(2012)46.
31. B. Yemu, ZSimpWin, Version 2.00 (Echem Software, Ann Arbor, 1999)